https://doi.org/10.5194/essd-2025-123
Preprint. Discussion started: 25 March 2025

Open Access Earth System Science Data Discussions

A full year of continuous net soil and ditch CO_2, CH_4, N_2O fluxes, soil hydrology and meteorology for a drained fen in Denmark

Annelie Skov Nielsen[1], Klaus Steenberg Larsen[1], Poul Erik Lærke[2], Andres Felipe Rodriguez[2], Johannes Wilhelmus Maria Pullens[2], Rasmus Jes Petersen[3], Jesper Riis Christiansen[1]

[1]Department of Geoscience and Natural Resource Management, University of Copenhagen, Frederiksberg, DK-2000, Denmark

[2]Department of Agroecology, Aarhus University, Tjele, DK-8830, Denmark
[3]Department of Ecoscience, Aarhus University, Aarhus, DK-8000, Denmark

Correspondence to: Jesper Riis Christiansen (jrc@ign.ku.dk)

Abstract. We here present a detailed dataset of automated greenhouse gas (GHG) net soil and ditch fluxes of carbon dioxide (CO_2), methane (CH_4), and nitrous oxide (N_2O) from a drained fen in Denmark covering a full year. The dataset resolves small scale spatial and hourly-daily-seasonal dynamics of GHG soil fluxes. The GHG flux dataset is accompanied by simultaneous time series of soil temperature and moisture, as well as groundwater table depth and covers spatiotemporal gradients in soil hydrological and climatic variability. The GHG fluxes of CO_2, CH_4 and N_2O were measured simultaneously by a high-precision cavity ring down laser spectrometer connected with a novel automated GHG system platform called SkyLine2D (Earthbound Scientific Ltd., UK) that allowed up to 27 individual chamber measurement points along a 24 meter transect. In total 47.483 chamber measurements were completed and after quality control 44.631 CO_2 fluxes, 44.099 N_2O and 42.515 CH_4 fluxes remained.

The average net soil CO_2 efflux observed at the site (2.55 µmol CO_2 m^{-2} s^{-1} or 35 tCO_2 ha^{-1} y^{-1}) aligns with findings from similar drained fens in northern Europe. However, this transect average masks substantial spatial variability and highlights the role of episodic emission bursts related to hydrological variability. N_2O fluxes measured at this site were similarly variable in space, but displayed a more dynamic flux behaviour than CO_2, where increasing groundwater table depth in response to precipitation during warmer seasons lead to emission bursts of N_2O that dominated the annual budget and decreased to near-zero fluxes in drier periods. Soil CH_4 fluxes were near-zero and the site overall acted as a small net source, although net uptake was observed as well especially in drier conditions.

Diurnal and seasonal patterns of net soil CO_2 and N_2O fluxes align with expectations of soil temperature driven processes, but no clear patterns were observed for CH_4. Compared to soil GHG fluxes, ditch CO_2 and N_2O fluxes were 4-fold and 27-fold lower, respectively, while CH_4 fluxes were more than two orders of magnitude larger, confirming earlier findings that ditches can be CH_4 hotspots, where the CH_4 is emitted in bursts with little seasonal variability, including emissions as ebullitions.

The data set is well suited for testing and developing biogeochemical models, with emphasis on the soil thermal-hydrology interactions with the peat C and N cycles.

https://doi.org/10.5194/essd-2025-123
Preprint. Discussion started: 25 March 2025

Open Access Earth System Science Data Discussions

1 Introduction

Understanding the climate feedbacks of temperate drained and rewetted wetlands require robust observational datasets of net fluxes able to capture spatial and temporal variability from these systems. Flux data covering all three major greenhouse gases (GHGs) are rare for temperate peatlands, and most of our understanding of flux dynamics in these ecosystems are either derived from eddy covariance systems that are unable to resolve small scale spatial drivers or temporally discrete manual GHG flux measurement that cannot be used to understand hourly-daily dynamics. In turn this hampers the ability to model and forecast GHG fluxes in these systems under land use and climatic change.

Automated GHG closed chamber flux measurements from ecosystems are becoming increasingly common as equipment costs decrease and awareness grows about the importance of resolving temporal variability of GHG fluxes to better understand soil biogeochemical processes and soil-climate feedback. Most automated chamber systems are setup around a multiplexer control unit linking multiple chambers with one or more analyzers. State-of-the-art automatic chamber systems, like the LI-8250 Automated Gas Flux System, allow for standard number of 8 chambers that can be upgraded to 36 chambers with additional manifolds. Such large replicate chambers allow for improved characterization of spatial variation or treatment effects coupled with temporal variations.

While the basic principles and assumptions of flux calculation from static closed chamber measurements were established over 40 years ago (Hutchinson & Mosier, 1981) the advent of automated chamber systems raises the need for improved data handling and flux calculation tailored to handle a wide range of flux magnitudes and chamber behaviour or design (Kroon et al., 2008; Pihlatie et al., 2013). Recent examples of novel flux calculation software are based on publicly available R codes and include goFlux (Rheault et al., 2024), HMR (Pedersen et al., 2010; Pullens et al., 2023) and fluxfinder (Wilson et al., 2024).

With unsupervised automated chamber flux measurements the likelihood of misinterpretation of fluxes increases, such as overestimated night-time fluxes (Brændholt et al., 2017) or leaky chambers that disturb chamber headspace concentrations. This is a significant challenge of automated chamber systems producing thousands of data points, where manual control of each data point may not be practical or feasible. Integrated quality control, flagging erroneous or uncertain flux measurements, enabling an objective filtering of poor quality data on the entire dataset are implemented in the most recent flux calculation R scripts.

The objective of this study is to present a dataset on net surface fluxes of carbon dioxide (CO_2), methane (CH_4) and nitrous oxide (N_2O) measured with an automated GHG chamber system over 12 months along a 24 m transect on a temperate drained fen peatland. High-frequency data of GHG fluxes are still scarce for peatlands and spatial variability is rarely represented as well. This dataset addresses some of these shortcomings and is published with the aim of it being used by the scientific community for exploring GHG dynamics in relation to hydrology and climate, as well as modelling.

https://doi.org/10.5194/essd-2025-123
Preprint. Discussion started: 25 March 2025

Open Access Earth System Science Data Discussions

2 Materials and Methods

2.1 Site description

The field site, Vejrumbro, is located in Central Jutland near the city of Viborg (Fig. 1). It is situated in the Nørre Å valley and is characterized as a riparian fen peat soil (Reza Mashhadi et al., 2024). The mean annual temperature is 8.3°C with mean annual precipitation of 675 mm over the period 1991–2022 (Aarhus University Viborg, Meteorological Station, Foulum). The site was drained in 1950 with ditches and tile drains for cultivation but has primarily served as grassland in recent decades due to the wet conditions (Nielsen et al., 2024). The riparian fen developed in a former glacial river valley with flat topography gently sloping (<2.5 meters over 300 meters) towards the Nørre Å that makes out the central river in this area (Fig. 2). Farming practices with tillage and crops stopped approximately 20 years ago after which it was managed as a harvested grassland (Thers et al., 2023). Since 2018, Vejrumbro has been a living lab for agroecological research managed by the Department of Agroecology at Aarhus University. From 2018, the site had a passive rewetting strategy by terminating maintenance of the open ditches. During 2022, the main ditches were gradually blocked. Currently, the area is being encroached by *Juncus effusus* except in few plots of the field where paludiculture research is taking place (Nielsen et al. 2024).

Figure 1: The Vejrumbro location in Jutland (N 56.43819 E 9.54527 (WGS 84)) in the Nørre Å valley near the village of Vejrumbro. The grey circle marks the placement of the SkyLine2D system. Satellite images: © Google Earth.

https://doi.org/10.5194/essd-2025-123
Preprint. Discussion started: 25 March 2025

Open Access Earth System Science Data Discussions

Figure 2: The Vejrumbro site looking south east towards Nørre Å. *Juncus effusus* plants are colonizing part of the area which is otherwise covered by grass.

https://doi.org/10.5194/essd-2025-123
Preprint. Discussion started: 25 March 2025

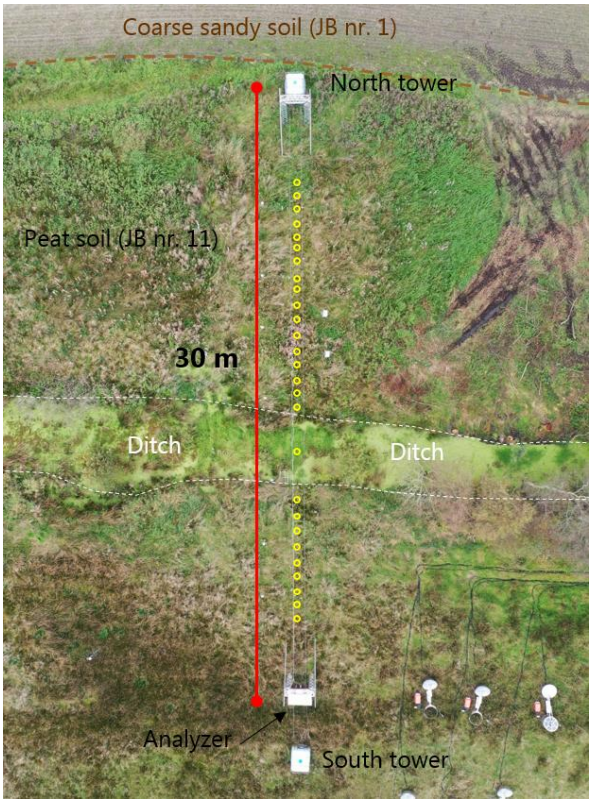

Figure 3: Drone image of the measurement transect (September 27th 2023) after flux measurements had stopped. Dashed brown line marks the approximate boundary between the agricultural field, coarse sandy soil (JB nr. 1 according to the Danish soil classification (north)) and the peat soil (JB nr. 11 according to the Danish soil classification (south)). The red line marks the end points of the SkyLine2D system (30 meters). The open yellow circles (n=27) mark the approximate position of individual collars across the transect of the field (22 meters in length) where greenhouse gas fluxes were measured. The ditch is indicated with dashed white lines. The analyser was placed at the south tower. Elevation along the 22 meter collar transect varied little across the transect from 3.77 m in the south to 4.06 m in the north.

The measurement transect was oriented in an N-S direction (Fig. 3). Two 2.5 meter-tall scaffold towers marked the end of the 30 m SkyLine2D system (Fig. 3 and 5D). The towers were fixed by ropes attached to 1000L pallet tanks filled with water (Fig. 5D). The measurement transect was in total 22 m with 27 individual measurement collars for GHG fluxes on the ground, 26 on peat and 1 in a drainage ditch (Fig. 3 and 4). The GHG analyzer was installed in a waterproof and temperature-controlled shelter at the south end of the transect (Fig. 3 and 5B). The transect was situated on the edge of the riparian fen in close proximity to the mineral upland soils, where active agriculture was practiced (Fig. 3). Along the transect volumetric soil water content (SWC) and soil temperature (ST) as well as water table depth (WTD) was measured at seven locations along the transect (Fig.

https://doi.org/10.5194/essd-2025-123
Preprint. Discussion started: 25 March 2025

Open Access Earth System Science Data Discussions

4). The farmer's field north of the SkyLine2D was sown with annual crops in rotation according to normal practice.

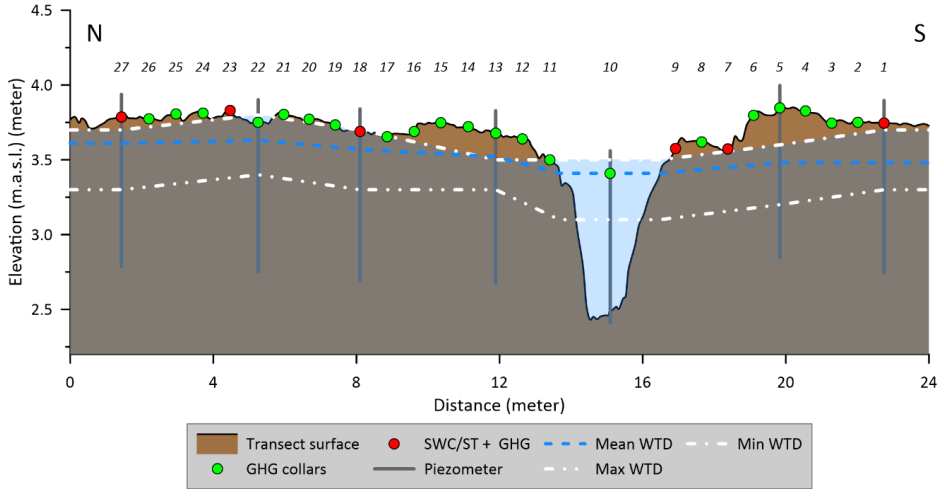

Figure 4: Schematic representation of the measurement transect at Vejrumbro and associated measurement variables. Mean WTD is the mean water table depth measured in piezometers (blue dashed line). GHG collars (green symbols) mark the positions of greenhouse gas flux measurements of CO_2, CH_4 and N_2O. SWC/ST + GHG mark the positions where volumetric soil water content (SWC) and soil temperature (ST) at 5 cm depth were measured alongside greenhouse gas fluxes. Numbers on top of plot show the collar numbers (from 1 – 27). N and S mark the north and south ends of the transect (see Fig. 3). The peat depth was at least one meter in all points. The lower depth of peat in the diagram is however arbitrary.

2.2 Data variables

The dataset is comprised of a 13-month time series of net soil fluxes of CO_2, CH_4 and N_2O, soil temperature and moisture at 5 cm depth, meteorological variables (air temperature, wind speed and direction measured at 2 meter height) and groundwater table level, depth and temperature (Fig. 4, Table 1). The GHG flux measurements started on August 1st 2021, with a data gap between September 1st 2021 and February 1st 2022 due to equipment failure (Table 1). Groundwater level measurements started between March 9th to 31st 2022 (Fig. 4, Table 1). All other variables were measured continuously from July 1st 2021 until January 31st 2023 (Fig. 4, Table 1).

Table 1: Available time series data from the Vejrumbro SkyLine2D system. Coloured time periods for each variable indicate data availability.

			Frequency (minutes)	2021					2022												2023
Variable	Unit	Model/sensor type		Aug	Sep	Oct	Nov	Dec	Jan	Feb	Mar	Apr	May	Jun	Jul	Aug	Sep	Oct	Nov	Dec	Jan
CO_2 flux[1]	µmol CO_2 m^{-2} s^{-1}	G2508 (Picarro Inc., USA)	~10[2]																		
CH_4 flux[1]	nmol CH_4 m^{-2} s^{-1}	G2508 (Picarro Inc., USA)	~10[2]																		
N_2O flux[1]	nmol N_2O m^{-2} s^{-1}	G2508 (Picarro Inc., USA)	~10[2]																		
Soil temperature at 5 cm depth[3]	°C	RXW-TMB-868 (Onset, USA)	5																		
Soil water content at 5 cm depth[3]	(cm^3 cm^{-3})	RXW-SMD-868 (5HS) (Onset, USA)	5																		
Air temperature at 2 m height	°C	S-THC-M002 (Onset, USA)	5																		
Wind speed	m s^{-1}	S-WSB-M003 (Onset, USA)	5																		
Wind direction	°	S-WDA-M003 (Onset, USA)	5																		
Groundwater level[4]	m.a.s.l.	DCL532 (BD sensors, Germany)	15																		
Groundwater table depth[4]	cm	DCL532 (BD sensors, Germany)	15																		
Groundwater temperature[4]	°C	Dallas DS 18B20	15																		

[1]Net soil/ditch fluxes.
[2]Time in between two consecutive flux measurements. The 10 minutes comprise actual flux measurement of 5 minutes and 5 minutes headspace flushing between flux measurements.
[3]Measured for a subset of collars: 1, 7, 9, 18, 23, 27.
[4]Measured for a subset of collars: 1, 5, 10 (ditch), 13, 18, 22, 27.

https://doi.org/10.5194/essd-2025-123
Preprint. Discussion started: 25 March 2025

2.3 Soil moisture and temperature measurements

Soil moisture probes were inserted at an approximate 30˚ angle 5 cm outside the collar, while the soil temperature probes were inserted vertically adjacent to the soil moisture probe.

2.4 Groundwater table level and depth

Piezometers (inner diameter 5 cm) were installed to 1 meter depth below the surface, which is deeper than the lowest groundwater level in summer (~60 cm below the surface) with openings from 0.1 – 1.2 meter below terrain. The piezometers were installed approximately 50-60 cm beside the collars to avoid interference with the SkyLine2D system. After installation, piezometers were cleaned and sealed at the surface with bentonite pellets to avoid surface infiltration along the piezometers which can distort water level measurements.

Pressure transducers (DCL532, BD Sensors, Germany) connected to Arduino-loggers were installed in each piezometer (at collars 1, 5, 10, 13, 18, 22 and 27 – Fig. 5) approximately 1 m below terrain collecting water levels every 15 minutes. The pressure transducers were vented, and thus do not need correction for atmospheric pressure.

The groundwater levels were described using two metrics: hydraulic head and groundwater depth (GWD). Hydraulic head represents the water level relative to mean sea level, based on the Danish Vertical Reference (DVR90), while GWD indicates the depth of the groundwater below the surface terrain. The elevation of top of the piezometers were measured using a GPS (model GS07 High Precision GNSS Antenna with a CS20 Controller, Leica, Germany) and used as a local reference for hydraulic head. Manual measurements of groundwater levels were conducted every 2 months and used to calibrate the logger water levels to hydraulic head and GWD.

2.5 Wireless data transfer

Wireless sensors for air temperature, wind speed, wind direction, soil temperature and volumetric soil water content were set up with Wi-Fi data transfer to HOBO RX3000 Weather Station (Onset, USA) equipped with HOBOnet Manager (RXMOD-RXW-868) module for wireless communication with sensors and logged data every 5 minutes. Data access was through the HOBOlink cloud software.

Groundwater loggers were interfaced with the I^2C (Inter-integrated Circuit) protocol and data was collected on Arduino custom-built logger (https://vandstande.dk/logger.php) with wireless connection via LoRaWANor SigFox.

2.6 Greenhouse gas flux measurements

2.6.1 SkyLine2D system at Vejrumbro

The SkyLine2D system is designed and built by Earthbound Scientific Ltd. (England). 27 individual collars (Ø19 cm) along the 22 meter transect (Fig. 3) were inserted 5 cm into the peat leaving 5 cm above the surface. The collars were distanced app. 70 cm apart. 1 collar was installed in the ditch by inserting a tube (Ø19 cm) to the bottom of the ditch with holes to allow water flow. On top of this longer tube a collar was glued to the top

https://doi.org/10.5194/essd-2025-123
Preprint. Discussion started: 25 March 2025

allowing for flux measurements. The chamber was programmed to stop when the bottom of the chamber hit the water surface if the water level in the ditch extended above the top of the collar. For the majority of the time the collar was not submerged and the chamber therefore hit the collar.

Prior to installation of collars in summer of 2021, the transect (Fig. 3) was harvested and remaining living aboveground vegetation was killed by applying one dose of Glyphosate across the transect. Subsequently, regrowth inside the collars was restricted by manual harvesting of emerging plants at a minimum of once every 7 days and throughout the period. Thus, the fluxes measured represent the net soil GHG flux.

2.6.2 Trolley and Chamber

There was one round transparent chamber (height: 39.5 cm and inner Ø: 19 cm, volume: 11.2 L) on the SkyLine2D, hanging below a moving trolley, which was suspended on two ropes stretched between the north and south towers (Fig. 5A and B). At defined positions along the rope, neodymium magnets had been inserted, and a magnet sensor (Fig. 5B) on the trolley informed the internal computer to stop and lower the chamber over positions with a collar on the surface. The chamber was lowered and guided down to the collar by supporting rods shaping a funnel (Fig. 5A). The chamber stopped when it hit the collar, achieved through a pressure sensor on top of the chamber connected to a hollow rubber gasket (Ø 3 cm) at the bottom, which also sealed the chamber with the collar. There was no fan installed in the chamber as the mixing was ensured by the main pump (Fig. 5C). A vent was installed in the top of the chamber to allow for pressure equilibration under windy conditions and chamber deployment.

Two signals from the internal computer in the trolley were logged on the RMX3000 datalogger during the time the chamber was on the collar: chamber closed (CH_closed) and chamber ID (CH_ID). CH_closed measured the cumulative time the chamber was in contact with the collar, while CH_ID was recorded as a voltage output dependent on the magnet number, starting with 0.05V for CH_ID 1. With 30 magnets in the rope, the maximum CH_ID value was 1.5. In this study, 27 out of the 30 magnets were used.

https://doi.org/10.5194/essd-2025-123
Preprint. Discussion started: 25 March 2025

Figure 5: A) The SkyLine2D trolley and chamber at Vejrumbro site looking from south towards the north tower. Note the orange collars on the ground arranged in a straight line. B) Close-up of the chamber: wheels move the trolley back and forth on the ropes (1), magnet sensors (2) and rubber gasket on the bottom of the chamber (3). C) The analyzer "hut" with the Picarro G2508 gas concentration analyzer (4) and the main pump (5). D) The SkyLine2D system with the north and south towers and the analyzer shelter. Towers were at both ends attached with ropes to water-filled 1000 L pallet tanks. One tank shown at the right of the picture.

2.6.3 Flux measurements

One entire flux + flushing sequence lasted 10 minutes (Table 1). The chamber closure period was set to 5 minutes with a purging time of 5 minutes in between measurements when chamber was open and hanging underneath the trolley at approximately 1 meter above the ground (Fig. 5D). This provided on average 10 min between flux measurements on consecutive collars (Table 1). Due to small variations in mechanical operations, flux measurements were occasionally farther apart than 10 minutes, but overall the timing of the SkyLine2D system was consistent. After each cycle of 27 flux measurements there was a 30-minute delay until the start of the next cycle. On average this resulted in 4-5 flux measurements per collar per day throughout the period.

To determine the concentrations of CO_2, CH_4 and N_2O in the chamber air, a laser spectroscopy analyzer (model G2508, Picarro Inc., USA) was used. The sample output frequency was set to 1 hz with a manufactured specified raw precision for CO_2: 240 ppb, CH_4: 0.3 ppb and N_2O: 5 ppb at ambient conditions (Picarro Inc., USA).

https://doi.org/10.5194/essd-2025-123
Preprint. Discussion started: 25 March 2025

A main pump (model: N86 KN.18, KNF, Germany) circulated the air to and from the chamber at 6 L min^{-1}. The G2508 gas analyzer was installed in parallel to the inflow from the chamber due to the much lower flow of 250 mL min^{-1} of the vacuum pump. There was a 30-meter tube between the chamber and main pump to allow for the analyzer to remain stationary in the "hut" while the trolley moved. This unavoidably created a delay in the chamber headspace GHG concentration of about 60 seconds after chamber closure.

The analyzer, vacuum pump and main pump were placed in an automatically ventilated wooden "hut" (Fig. 5C). An overview of the SkyLine2D system in place is shown in Fig. 5D.

2.7 Calculation of diffusive fluxes

Fluxes were calculated and quality checked using the procedure outlined in the goFlux R package (Rheault et al., 2024). The CO_2, CH_4 and N_2O concentrations in ppm were converted to moles using the ideal gas law.

Prior to flux calculations, the gas concentration data from the G2508 was matched to the CH_closed and CH_ID time series in order to determine the start time of the chamber measurement, so it was possible to separate individual flux measurements from each collar over the measurement time (see examples of flux detection and calculation in Fig. 6A-D). An automatic deadband detection method was applied based on maximal R^2 of a linear regression over the first 180 s (in 10 s steps) after chamber closure. The deadband was allowed to attain values between 0 to 150 seconds thereby also allowing for compensation for the ~60 s delay between chamber headspace gas concentration change and G2508 analyzer detection due to transport time through the 30 m tube connecting the chamber and analyzer.

Flux calculations were done with both linear (LM) and non-linear (Hutchinson-Mosier – HM) regression models (Pihlatie et al., 2013) to determine the slope at time zero. The best flux estimate with either the LM or HM regression model was determined using the *best.flux* function in the goFlux package (Rheault et al., 2024). Shortly, if the RMSE of the HM model was lower than minimum detectable flux (MDF), HM was chosen. However, if the ratio (g-factor) between HM and LM was larger than 2, LM was chosen, as this indicates over-fitting of the HM, which may result in unrealistic large HM flux estimates. If the relative SE of the slope (SE/slope) at time zero for the HM model was larger than 100% than the SE of the LM it also indicated overfitting and the LM was chosen. This approach is conservative as it will discard non-linear flux behaviour and instead provide a conservative linear flux estimate. Out of 47.438 detected flux measurements for CO_2, CH_4 and N_2O, respectively, a total of 2807 CO_2 fluxes (5.9%), 3339 N_2O fluxes (7%) and 4923 CH_4 fluxes (10.3%) were discarded due to chamber mechanical malfunction (imperfect sealing on collar or erroneous lowering of chamber on collar) and non-significant regression due to noisy measurements at low flux levels. For flux measurements the air temperature in 2 meters was used as an estimate of the chamber headspace temperature along with a 1 atm air pressure.

The annual budget of fluxes from the soil or the ditch was estimated simply by multiplying the daily average CO_2, CH_4 or N_2O flux for the measurement period with 365 days. We believe for the purpose of data presentation that this simplistic methodology is adequate here, also given the very few data gaps in the timeseries. However, there are other more sophisticated methods using interpolation and response variable

https://doi.org/10.5194/essd-2025-123
Preprint. Discussion started: 25 March 2025

functions that may refine the annual budget. However, it is not the goal of this manuscript to present these methodologies but to provide the data so other users can test different temporal upscaling methodologies.

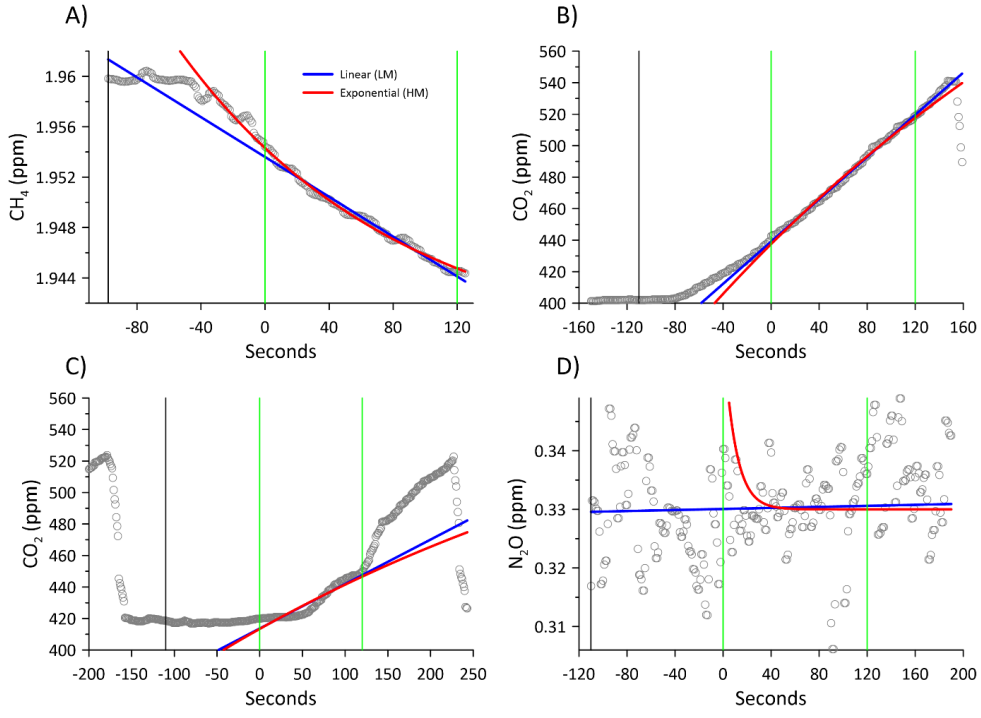

Figure 6: Example of flux detection and resulting flux calculation using linear (blue) (LM) and non-linear (red) (HM) regression models. Chamber closure is marked by the black vertical line and the 120 second flux calculation window marked by the green vertical lines. Examples of successful measurements of A) net CH_4 uptake measurement, B) CO_2 efflux, C) example of erroneous detection of chamber closed and D) example of measurement of non-detectable N_2O flux with HM overfitting.

Due to a combination of variability in flux magnitudes and the mechanics of the SkyLine2D it is possible to achieve a number of situations where fluxes will be discarded. Successful flux measurements and calculations are when the timing of chamber closed and GHG time series are synchronized (Fig. 6A and B). As seen from the numbers in the previous paragraph this was the case in more than 90% of all flux measurements. However, if there was a mismatch between the chamber closed detection and the time series of GHG concentrations the flux would be calculated on a wrong "window" of the actual enclosure (example in Fig. 6C). This window could either be too early or late and fluxes would accordingly be discarded. Lastly, at low fluxes, but otherwise successful deployment of the chamber, the HM model could overfit the GHG time series and result in unrealistic flux estimates (Fig. 6D). In this case flux calculations would also be discarded.

2.8 Calculation of ebullition fluxes in the ditch

Ebullition, e.g. mass flow of CH_4, was occasionally observed only in the ditch. The resultant CH_4 time series for the chamber would have a characteristic appearance (Fig. 7) where the measurement would essentially start out

https://doi.org/10.5194/essd-2025-123
Preprint. Discussion started: 25 March 2025

as diffusive flux measurement, then CH_4 bubbles entered the chamber headspace and the concentration would quickly increase to a maximum value and reach a threshold concentration corresponding to the mixed headspace concentration. In these cases the LM/HM flux calculation assumptions are violated and instead the ebullition flux would be calculated as the total increase in CH_4 mass m^{-2} $enclosure^{-1}$. The mass flux of CH_4 per enclosure (nmol m^{-2} $enclosure^{-1}$) was calculated according to Eq. (1):

$$F_{CH_4-ebu} = dCH_4 * \frac{V_{system}*P}{A*R*T} * 10^{-6} \quad (1)$$

Where dCH_4 is the concentration difference in nmol between start of chamber enclosure ($CH_{4,start}$) and end CH_4 concentration ($CH_{4,end}$) after it reached a plateau (Fig. 7), V_{system} is the total volume (11.7 L) of the system (collar, chamber, tubes and analyzer) in L, P is the pressure (1 atm), A is the area of the collar (0.028 m^2), R is the gas constant (0.082057 L atm K^{-1} mol^{-1}) and T is the chamber headspace temperature (K).

As the fluxes from the ditch were only measured 4-5 times per day (every 5-6th hour), the measured ebullition fluxes were upscaled to daily basis under the assumption that the frequency of ebullitions were constant during 24 hours. This may not be the case as ebullition fluxes from open water surface (Sø et al., 2023; Wik et al., 2016) are known to be erratic. However, ebullition would happen also from the ditch when the flux was not measured, so upscaling ebullition on a daily basis is the best estimate. The total ebullition flux from the ditch was upscaled to daily basis by multiplying the daily average measured ebullition flux per enclosures of 5 min with the number of possible 5 min enclosures in 24 hours (e.g. 24 *60/5).

For example on April 6th 2022 two ebullition fluxes were calculated (538 and 266 nmol CH_4 m^{-2} 5 min^{-1}, average of 402 nmol CH_4 m^{-2} 5 min^{-1}). To upscale to a daily basis the average value was multiplied by the number of 5 min enclosures in 24 hours, e.g. 402*24*60/5 = 115822 nmol CH_4 m^{-2} d^{-1}.

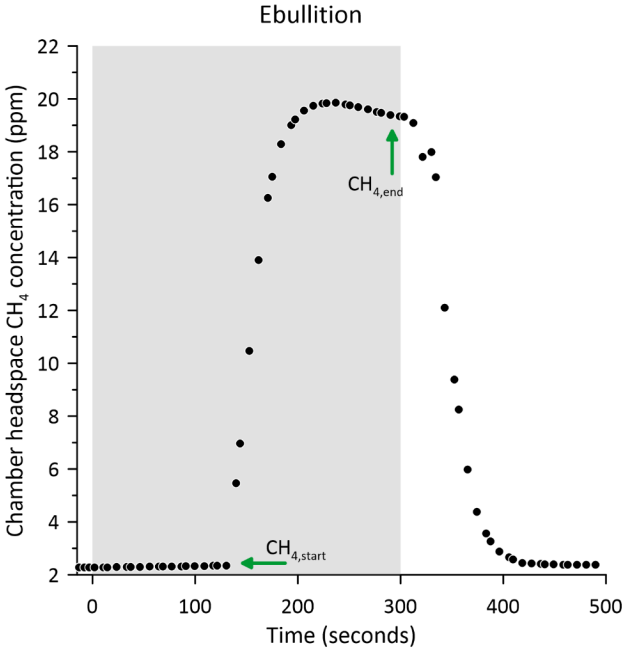

Figure 7: Example of ebullition measurement in the chamber.

Ebullitions could also be caused by mechanical disturbance of the chamber landing on the collar. Ebullition fluxes were discarded if the sudden increase in CH_4 headspace concentration (Fig. 7) occurred 30 seconds after recorded chamber closure as this indicated bubbles released by chamber deployment on top of the collar.

https://doi.org/10.5194/essd-2025-123
Preprint. Discussion started: 25 March 2025

Open Access Earth System Science Data Discussions

3 Data presentation

3.1 Wind speed and direction

Generally, the wind climate during the measurement period was rather mild with monthly average wind speeds ranging between 1.2 to 2.9 m s^{-1} and max gust up to 20 m s^{-1} (Fig. 8A). There was a typical seasonal behaviour of wind speed from winter to summer and an increase again towards the autumn (Fig. 8A) as is typically experienced in Denmark. The wind direction was uniformly from the west for 52% of the time, with easterly winds constituting 27% and northern and southern winds 8 and 13% of the time (Fig. 8B). Winds from western directions were highest for the longest period of time, while easterly winds were of similar magnitude, but less frequent (Fig. 8B). Northern and southerly winds were generally below 3 m s^{-1} and represented periods with still conditions. The dominance of direction and magnitude from a western direction is in line with the general wind direction in Denmark. The very uniform western-eastern wind field at Vejrumbro may also partly be explained by the W-E direction of the valley in which the site is situated, that effectively blocks or dampens winds from S and N.

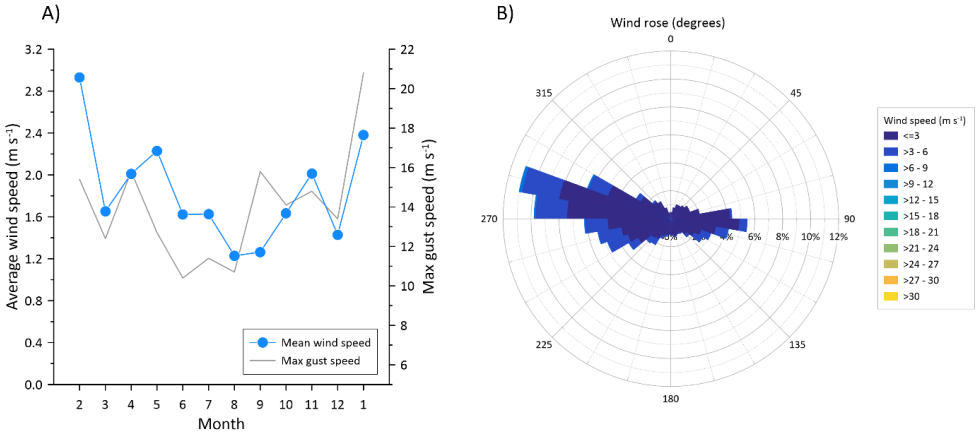

Figure 8: Wind climate at Vejrumbro for the period July 1st 2021 to January 31st 2023 A) average monthly wind speed (m s^{-1}) and maximum wind gust, B) wind rose diagram with wind speed and direction for the period.

https://doi.org/10.5194/essd-2025-123
Preprint. Discussion started: 25 March 2025

3.2 Air temperature

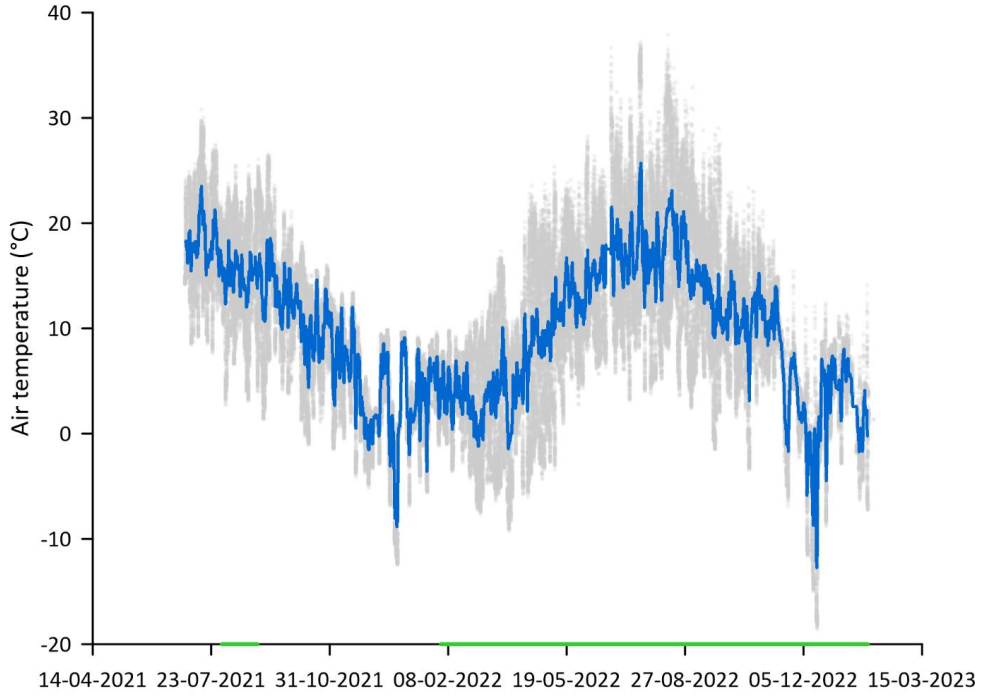

Figure 9: Time series of air temperature in °C measured at 2 meter height above the surface. The grey dots are the raw 5 min measurements of air temperature and the blue line represents daily means. The periods of GHG measurements with the SkyLine2D system are shown (green lines) on the x-axis.

The air temperature at Vejrumbro displayed typical seasonal variation for Danish conditions (Fig. 9). Over the study period the average air temperature was 9.6°C ranging between maximum 37.9°C and minimum of -18.6°C. Monthly mean, maximum and minimum temperatures shown in Table 2 show that the climate at Vejrumbro is quite dynamic with every month, except February, experiencing >20°C fluctuating between minimum and maximum temperatures pointing to large diurnal variations.

https://doi.org/10.5194/essd-2025-123
Preprint. Discussion started: 25 March 2025

Open Access Earth System Science Data Discussions

Table 2: Monthly mean, maximum and minimum air temperature and soil temperature (°C), groundwater table depth (cm) and volumetric soil water content (cm^3 cm^{-3}) at Vejrumbro in the measurement period from February 1st 2022 to January 31st 2023.

Variable	Year	2022											2023	
	Month	Feb	Mar	Apr	May	Jun	Jul	Aug	Sep	Oct	Nov	Dec	Jan	Avg
Air temperature (°C)	Mean	3.8	3.0	6.6	12.0	15.4	17.7	16.6	13.4	10.7	6.9	1.2	3.7	9.6
	Max	10.6	17.4	23.7	25.3	36.7	37.2	37.9	32.9	23.3	18.4	12.4	14.1	-
	Min	-4.3	-9.3	-8.3	-3.4	4.3	3.2	2.7	-1.5	-3.5	-6.9	-18.6	-7.3	-
Soil temperature (°C)	Mean	3.0	3.2	2.9	6.4	12.3	16.1	18.4	17.0	13.8	10.3	7.2	2.1	9.6
	Max	6.5	5.3	9.1	12.5	18.8	25.1	27.0	24.7	19.3	14.3	12.6	6.3	-
	Min	0.3	1.1	0.4	0.8	6.6	10.7	12.4	11.8	7.0	4.0	2.1	0.0	-
Groundwater table depth (cm)	Mean	-	39	35	41	36	41	35	31	20	18	17	13	29
	Max	-	58	39	58	43	52	46	36	30	31	28	28	-
	Min	-	23	5	24	9	28	22	9	5	6	3	2	-
Volumetric soil water content (cm^3 cm^{-3})	Mean	0.53	0.45	0.40	0.37	0.38	0.43	0.43	0.45	0.50	0.53	0.52	0.51	0.46
	Max	0.56	0.51	0.50	0.41	0.47	0.55	0.56	0.56	0.57	0.58	0.56	0.57	-
	Min	0.43	0.39	0.37	0.33	0.32	0.26	0.32	0.35	0.40	0.47	0.42	0.34	-

https://doi.org/10.5194/essd-2025-123
Preprint. Discussion started: 25 March 2025

3.3 Soil temperature

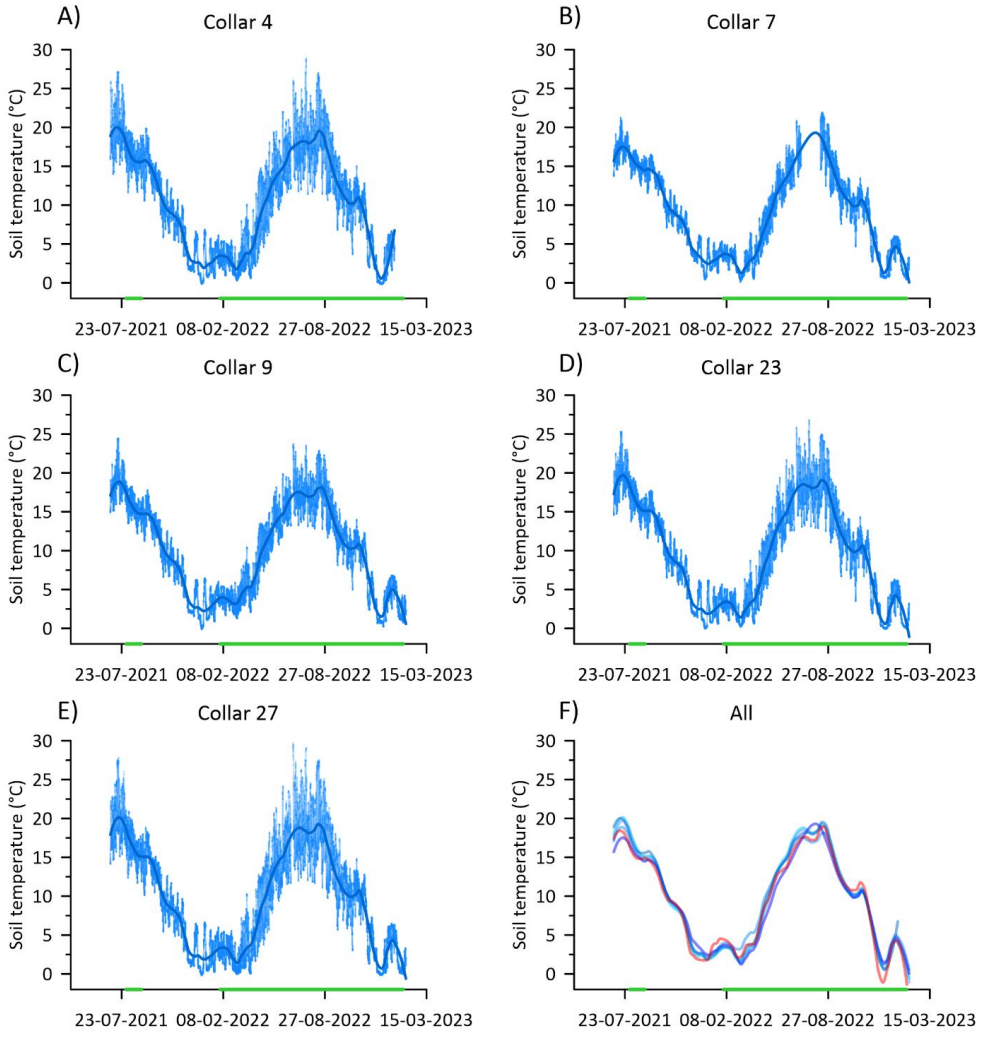

Figure 10: Time series of soil temperature (°C) at 5 cm depth for collars 4, 7, 9, 23 and 27 along the measurement transect at Vejrumbro. Solid blue line in plots are LOESS fit to show overall trend. Lower right panel compares overall trends of soil temperatures to air temperature (red line). Lines are LOESS fit of above graphs and raw data of air temperature (Fig. 7). The periods of GHG measurements with the SkyLine2D system are shown (green lines) on the x-axis.

Soil temperature magnitude and temporal variation was similar across the transect, varying between 0 to 28°C (Fig. 10A-E). The period of GHG flux measurements covered the entire seasonal variation in soil temperature. The seasonal variation of soil temperature followed that of air temperature (Fig. 10F) with less variability in temperature as expected both daily and seasonally (Fig. 10A-E and Table 2). The annual site average soil temperature was similar to the air temperature (Table 2).

https://doi.org/10.5194/essd-2025-123
Preprint. Discussion started: 25 March 2025

3.4 Water table depth (WTD)

Average WTD below terrain during the period was between 47 to 21 cm across the transect (Fig. 4, Table 2). During summer, the peat drained between 18 – 31 cm below the annual average and in winter the WTD increased to 0 – 22 cm above the annual average across the transect (Fig. 4, Table 2). Generally, the WTD was lower in the ditch across the entire study period (Fig. 4). It was only on the northern end of the transect that the surface occasionally was flooded during winter periods (Fig. 4).

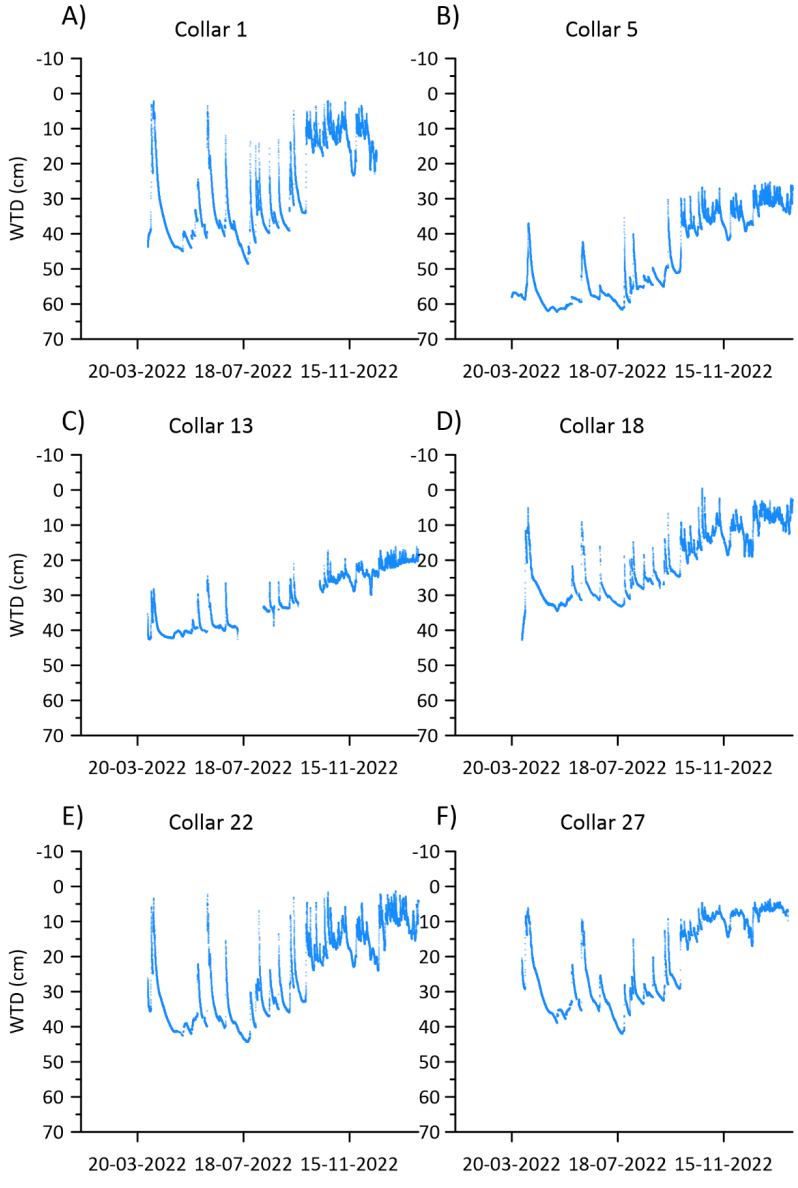

Figure 11: Time series of groundwater table depth (WTD) below terrain for the six piezometer locations along the SkyLine2D transect in the period 31.03.2022 – 31.01.2023 when the flux measurements stopped.

https://doi.org/10.5194/essd-2025-123
Preprint. Discussion started: 25 March 2025

Generally, the WTD displayed similar temporal variation despite different absolute water table depths (Fig. 11A-F). In the summer periods, the WTD was most variable decreasing to below -40 for collars 1, 13, 18, 22 and 27, whereas the WTD for collar 5 showed the deepest groundwater measured at the site. WTD responded quickly (within hours) to precipitation events that could increase the WTD by almost 40 cm at some plots, indicating that the entire aerated soil volume above the groundwater table was flooded. There was a slight tendency to lower response to precipitation events for piezometers at collar 5 and collar 13 that were placed closer to the ditch (Fig. 4 and 11B, C). As the ditch water level was lower than in the peat this could be explained by more efficient lateral drainage into the ditch from the areas closer to the ditch. In the winter periods, the WTD was less responsive to precipitation and was closer to the surface (Fig. 11A-F) across the transect.

https://doi.org/10.5194/essd-2025-123
Preprint. Discussion started: 25 March 2025

3.5 Soil water content

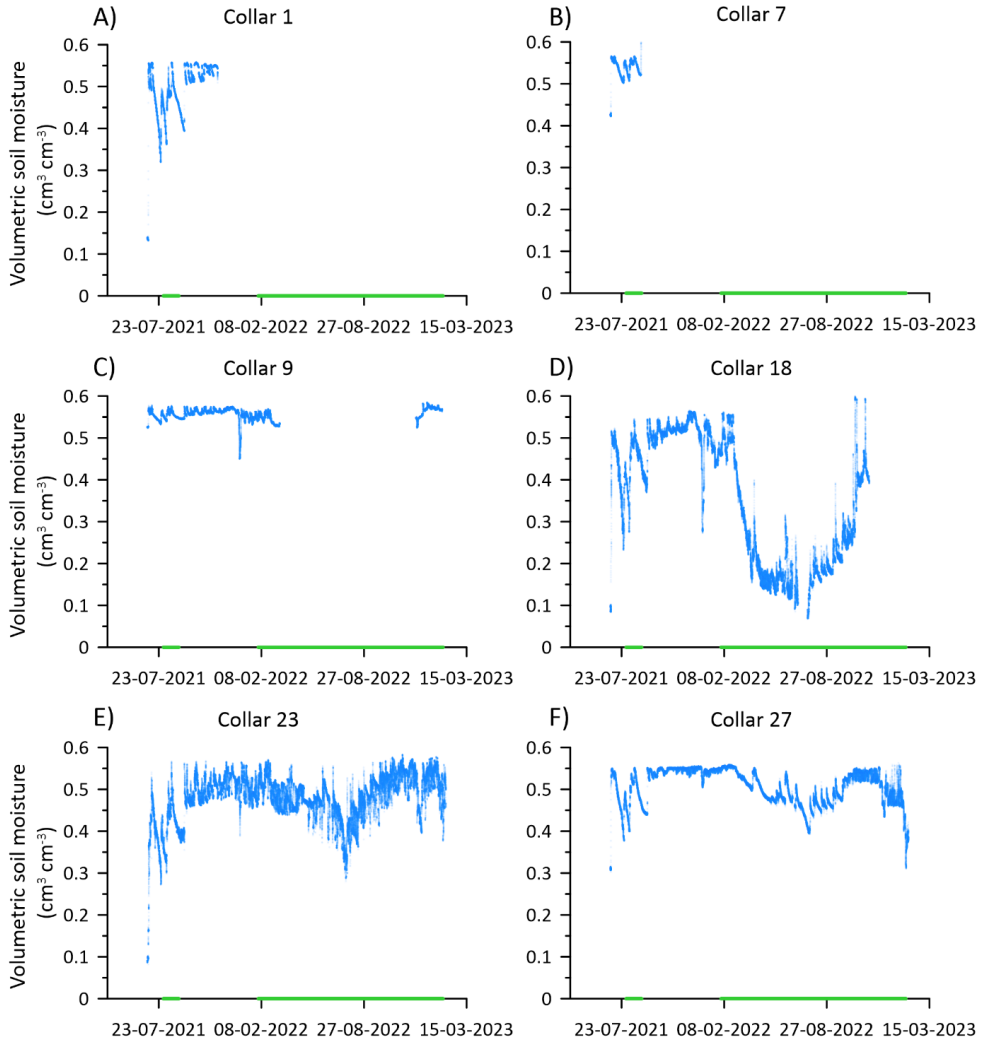

Figure 12: Time series of volumetric soil water content ($cm^3\ cm^{-3}$) in 0-5 cm for the six collars 1, 7, 9, 18, 23 and 27 along the SkyLine2D transect in the period 01.07.2022 – 31.01.2023 when the measurements terminated. The periods of GHG measurements with the SkyLine2D system are shown (green lines) on the x-axis.

Due to instrument failure the temporal coverage of soil moisture in the top soil (5 cm) was not similar across the transect (Fig. 12A-F). For collars 18, 23 and 27 the entire period of greenhouse gas measurements was covered by soil moisture measurements (Fig. 12D-F). While SWC for collars 1, 9, 18, 23 and 27 was similar in the winter periods (around 0.55 $cm^3\ cm^{-3}$) the SWC for collar 18 decreased to lower minima between 0.1 – 0.2 $cm^3\ cm^{-3}$, than the minima observed between 0.3 – 0.4 $cm^3\ cm^{-3}$ for collars 23 and 27 in the summer periods (Fig. 12, Table 2). Similar for all collars it was observed that SWC was more variable in summer, responding similarly as WTD to precipitation events (Fig. 12, Table 2). Since plants were removed regularly from the collars the

https://doi.org/10.5194/essd-2025-123
Preprint. Discussion started: 25 March 2025

decrease of SWC for collar 18 cannot be explained by plant transpiration, and the dynamic behaviour could indicate the impact of soil evaporation, but the different levels of SWC also show that there is spatial variation across the transect in the drying properties of the soil. However, it cannot be ruled out that the SWC sensor at collar 18 experienced malfunction or that soil contact was lost in the dry periods of 2022 (Fig. 12D) which could lead to erroneous and too low SWC. Therefore, these data should be considered with care.

3.6 Net soil and ditch CO_2, CH_4 and N_2O fluxes

3.6.1 Spatial variation of net soil CO_2, CH_4 and N_2O fluxes

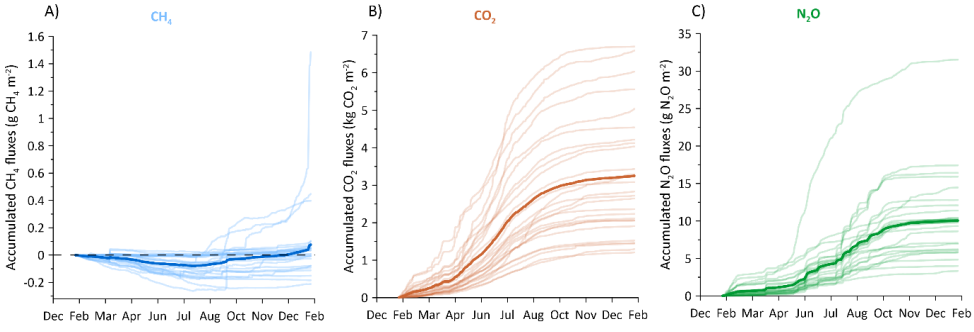

Figure 13: Cumulative fluxes of A) CH_4, B) CO_2, and C) N_2O for 26 individual collars along the SkyLine2D transect. Units for CH_4 and N_2O are in g CH_4/N_2O m^{-2} and for CO_2 in kg CO_2 m^{-2}. The cumulative fluxes represent the raw dataset. The ditch data was excluded. Site average is shown as thick lines.

Within the transect, cumulative CH_4 fluxes varied between -0.21 to 1.48 g CH_4 m^{-2} over the study period, with a site average cumulative flux of 0.07 g CH_4 m^{-2} (Fig. 13A and 14). Out of the 26 collars, excluding the ditch collar, 11 displayed a net uptake over the measurement period and the remaining were small net emitters (Fig. 13A and 14). There was generally little spatial variation in the absolute CH_4 fluxes among the soil collars, but three collars (11, 12 and 15) showed increasing net positive cumulative fluxes towards the ditch (Fig. 14).

The CO_2 effluxes displayed tremendous spatial variation across the 24-meter transect (Fig. 13B and 14) and measurements indicated that the drained peat soil was a net source of CO_2, with cumulative fluxes ranging between 1214 – 6740 g CO_2 m^{-2}, and a site average of 3269 g CO_2 m^{-2}, over the study period (Fig. 13B and 14). There was no apparent relation between the magnitude of cumulative CO_2 efflux to the position along the transect and average WTD (Fig. 14).

Similarly, the site was overall a net source of N_2O, with cumulative fluxes ranging between 3.3 – 32 g N_2O m^{-2}, with a site average of 10.1 g N_2O m^{-2} (Fig. 13C). Thus, there is a 10-fold difference between minimum and maximum cumulative N_2O fluxes within the transect, without any apparent relation to the position along the transect and WTD. The highest cumulative N_2O fluxes occurred at collar 8 situated close to the ditch (Fig. 14).

https://doi.org/10.5194/essd-2025-123
Preprint. Discussion started: 25 March 2025

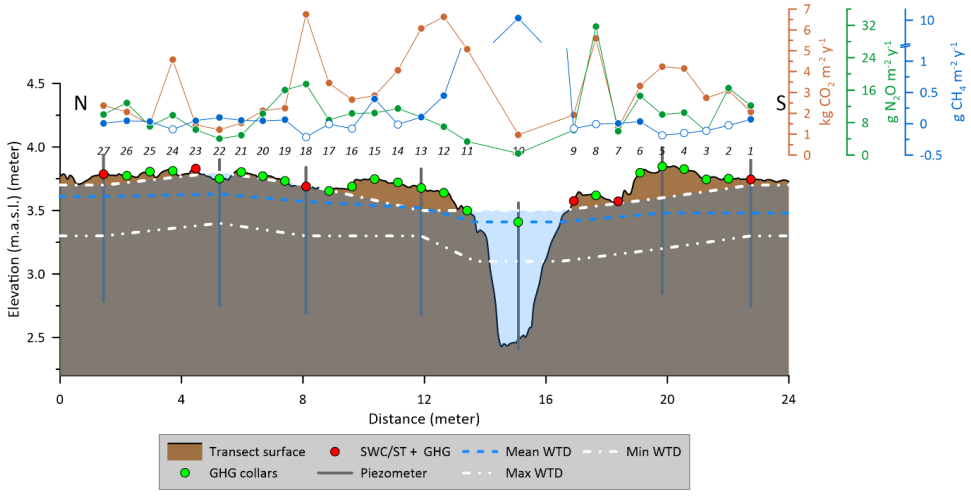

Figure 14: The annual cumulative fluxes of CO_2 (red) (kg CO_2 m^{-2} y^{-1}), N_2O (green) (g N_2O m^{-2} y^{-1}) and CH_4 (blue) (g CH_4 m^{-2} y^{-1}) over the measurement transect at Vejrumbro. Closed and open symbols for CH_4 represent net cumulative emission and uptake, respectively.

https://doi.org/10.5194/essd-2025-123
Preprint. Discussion started: 25 March 2025

3.6.2 Temporal variability of net soil CO_2, CH_4 and N_2O fluxes

3.6.2.1 Time series of raw data of net soil CO_2, CH_4 and N_2O fluxes

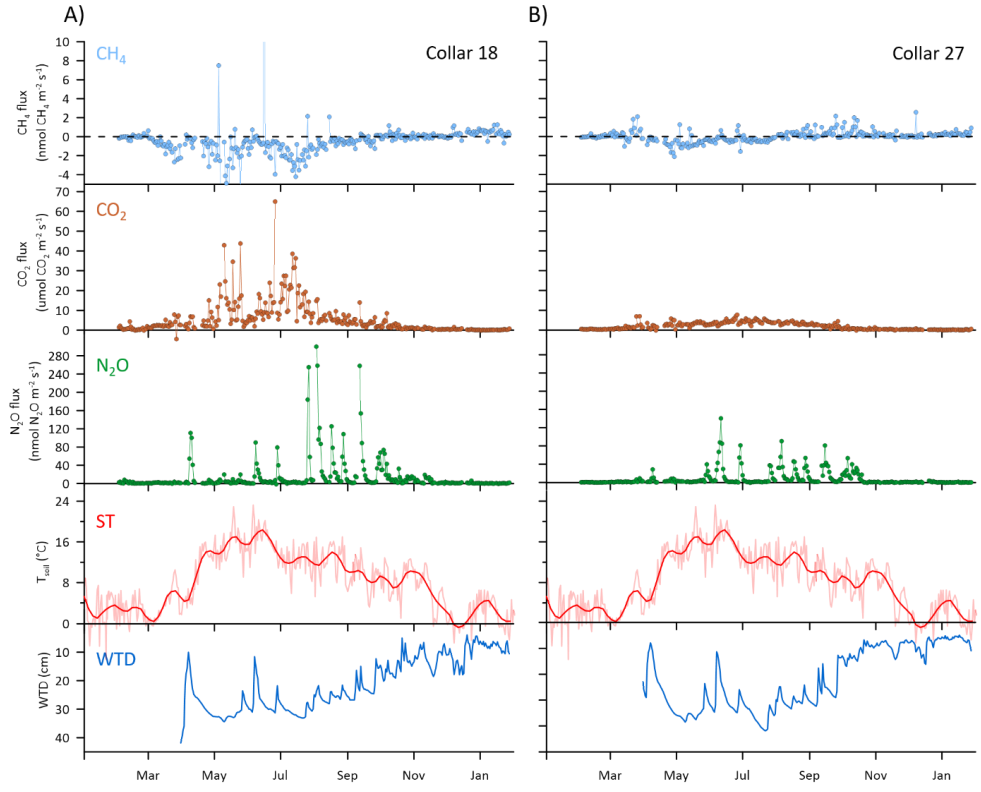

Figure 15: Examples of daily average time series of CH_4, CO_2 and N_2O fluxes for collars 18 and 27 at the SkyLine2D transect in Vejrumbro. soil temperature (ST)(°C) and groundwater table depth (WTD) in cm below terrain is shown in two lower panels.

With the high frequency of GHG flux measurements (on average 5 measurements per day per collar) it was possible to observe short term flux phenomena that in most studies deploying manual chambers are missed or if captured can lead to biased conclusions on flux magnitudes. For example, in most of the measurement points, CH_4 fluxes were generally near zero, but occasionally displayed elevated net emission for short periods even in periods with deeper WTD (Fig. 15A) for most chambers (see supplementary Fig. S1). This flux dynamic might be related to episodic release of CH_4 from deeper soil layers that are not fully oxidized in the aerated root zone (Askaer et al., 2011). As plants were not included in the collars these bursts cannot be attributed to plant emission pathways.

For net soil CO_2 fluxes the short-term flux dynamics differed between chambers (Fig. 15A and B). Often it was observed that soil CO_2 fluxes would show a seasonally increasing flux superimposed by rapid, within hours,

https://doi.org/10.5194/essd-2025-123
Preprint. Discussion started: 25 March 2025

burst (Fig. 15A), while other collars at the same period did not display this behaviour (Fig. 15B). This dynamic points to different emission pathways from the soil not related to plant mediated transport.

For N_2O, the spatiotemporal pattern was even more pronounced with N_2O generally across the transect being emitted in burst related to rapidly increasing or decreasing WTD that coincided with precipitation events. In drier periods with deeper WTD and little fluctuations, N_2O fluxes quickly dropped to near zero (Fig. 15A and B). Despite N_2O being emitted in similar temporal patterns across the site, the magnitude of the N_2O peaks were not similar across the transect (Fig. 15 and supplementary Fig. S1). Hence, the majority of N_2O is emitted in hot moments driven by fluctuations in WTD mainly (Fig. 15). In a dry forest ecosystem similar temporal patterns of N_2O fluxes have been found, but albeit driven by different soil physicochemical mechanism (Butterbach-Bahl & Wolf, 2017).

3.6.2.2 Diurnal variation of net soil CO_2, CH_4 and N_2O fluxes

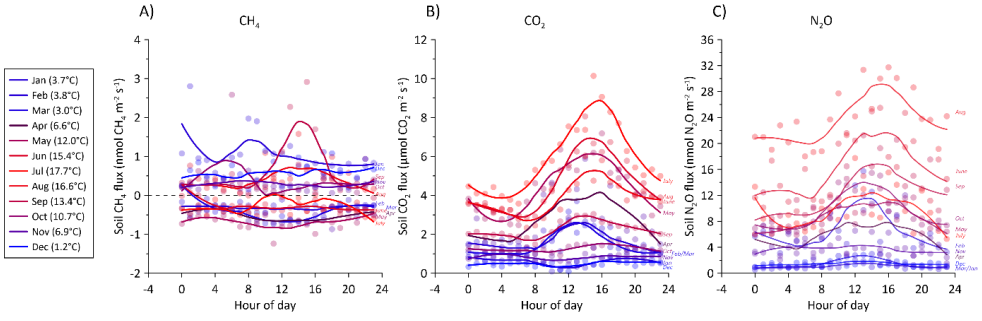

Figure 16: Average hourly flux for A) CH_4, B) CO_2, and C) N_2O during 24 hours for all the soil collars. Color shade between blue and red corresponds to average monthly air temperature shown in parenthesis in the figure legend. Solid lines are loess fits for visualization of the diurnal variation.

With the SkyLine2D system we observed diurnal variation for CO_2 and N_2O fluxes, but not for CH_4 (Fig. 16A-C). The amplitude of diurnal variability increased with higher air temperature for CO_2 (Fig. 16B) and partly for N_2O (Fig. 16C) with the month of July as an exception as it resembled the pattern observed in May although soil temperature was about 5°C higher in July than in May (Table 2). The lower N_2O fluxes observed in July can be attributed to lower and more constant WTD in July compared to May, June and September (Fig. 11).

https://doi.org/10.5194/essd-2025-123
Preprint. Discussion started: 25 March 2025

3.6.2.3 Monthly variability of net soil GHG fluxes

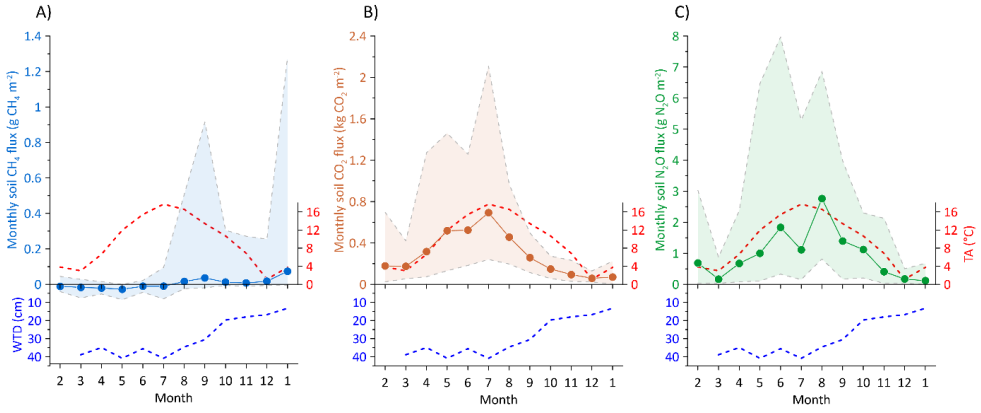

Figure 17: Monthly summed soil fluxes of A) CH_4 in g CH_4 m^{-2}, B) CO_2 in kg CO_2 m^{-2}, and C) N_2O in g N_2O m^{-2}. Shaded areas for CH_4, CO_2 and N_2O graphs represent the maximum and minimum monthly average fluxes. Blue dashed line below CH_4, CO_2 and N_2O represent the measured monthly average transect groundwater table depth (WTD) in cm below terrain. Red dashed line shows the monthly average air temperature (TA).

The soil GHG fluxes were summed to monthly transect average sums to illustrate long term drivers on the flux magnitude. Overall, fluxes relate both to temperature increase and lowering of the ground water table (Fig. 17). The lowest seasonal response was observed for CH_4 (Fig. 17A) where the flux was generally around zero. Net uptake increased slightly with increasing temperature and lower WTD during the spring and summer. With increasing water table and high temperatures in August the site turned into a small net CH_4 source continuing in fall and winter (Fig. 17A).

For CO_2 the seasonal variation was pronounced and closely followed soil temperature until peak values in July for both site average, minimum and maximum fluxes, respectively (Fig. 17B). From July to August it was observed that WTD at the site began to increase again and CO_2 fluxes departed from the close relation to soil temperature, indicating an inhibitory role of the WTD in this period, but reaching minimum fluxes in December, corresponding to the wettest and coldest month (Fig. 17B).

Similarly, N_2O fluxes increased with soil temperature reaching peak monthly values in August, corresponding to the period of the year with highest soil temperature and increasing WTD (Fig. 17C). This supports the promoting role of soil water saturation on the production of N_2O when temperature is favourable for denitrification. N_2O fluxes reached minimum values in December when WTD and ST were lowest (Fig. 17C).

https://doi.org/10.5194/essd-2025-123
Preprint. Discussion started: 25 March 2025

3.6.3 Ditch CO_2, CH_4 and N_2O fluxes

3.6.3.1 Time series of raw data of ditch CO_2, CH_4 and N_2O fluxes

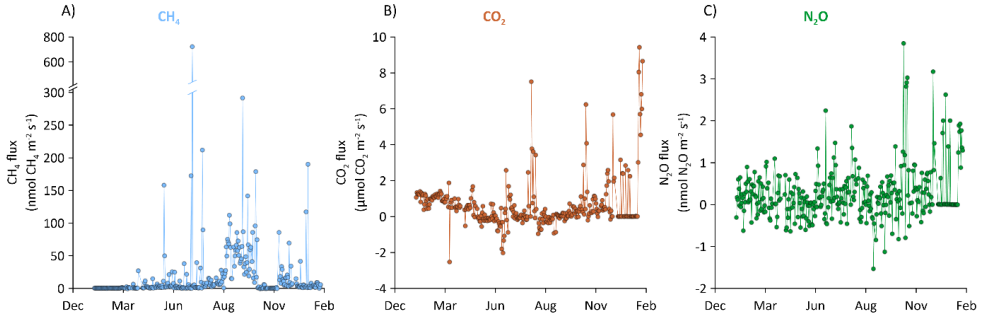

Figure 18: Daily average time series of net ditch total A) CH_4 (diffusion and ebullition), B) CO_2, and C) N_2O fluxes at the Vejrumbro site.

Common for all three gases is that ditch emissions are dynamic and net fluxes change from zero to large net positive or negative fluxes within hours or days (Fig. 18A-C). Methane is most dynamic with maximum flux close to 700 nmol CH_4 m^{-2} s^{-1}. There was a tendency toward consistently higher net CH_4 emission from August to September, becoming close to zero in colder seasons (Fig. 18A). Ebullition of CH_4 did occur occasionally in the ditch, but according to the flux calculation methodology and flux separation, diffusive fluxes dominated. However, it cannot be ruled out that the classification as diffusive flux may in fact be ebullition by nature. It has been suggested (Prairie & del Giorgio, 2013) that microbubbles resulting from mass transport can resemble diffusive fluxes in a chamber making it difficult, if not impossible, to fully separate the two emission mechanisms in a continuous time series if headspace CH_4 concentrations do not abruptly increase, such as in the example shown in Fig. 7. Hence, here the CH_4 fluxes are represented as total CH_4 flux, i.e. the sum of diffusive and ebullition. Compared to net soil CH_4 fluxes the ditch can be considered an emission hotspot at the site (10.4 g CH_4 m^{-2} y^{-1}), but fluxes are lower than earlier reports for ditches in other drained wetlands (between 0.1 – 44.3 g CH_4 m^{-2} y^{-1}) (Peacock et al., 2021).

For CO_2, there was a general tendency towards lower fluxes during the summer months and fluxes increased in magnitude and variability towards the end of the study period (Fig. 18B). For N_2O, the fluxes fluctuated around zero for most of the study period, except towards the end (December and January) where net fluxes became positive (Fig. 18C).

Compared to the net soil N_2O and CO_2 fluxes the ditch fluxes of these gases are low showing that the ditch is not contributing significantly to the CO_2 and N_2O budget at this site.

https://doi.org/10.5194/essd-2025-123
Preprint. Discussion started: 25 March 2025

3.6.3.2 Diurnal variability in ditch fluxes

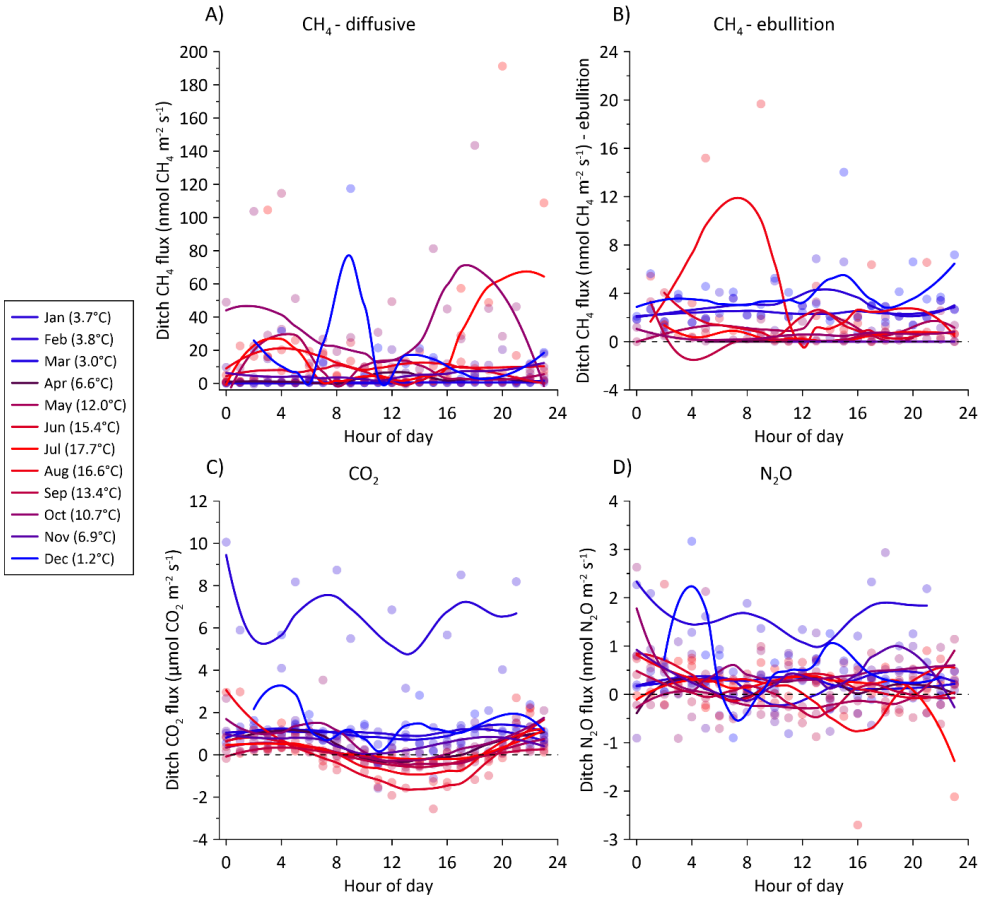

Figure 19: Average hourly flux for A) CH_4 diffusive fluxes, B) CH_4 ebullition fluxes, C) CO_2, and D) N_2O during 24 hours from the ditch. Colours correspond to average monthly air temperature shown in parenthesis in the figure legend. Note different axes.

For CH_4 fluxes, both diffusive and ebullition, there was no clear diurnal variability in any month (Fig. 19A and B). For net CO_2 fluxes from the ditch there was no diurnal variability in colder seasons (Jan, Feb, Mar, Nov and Dec), but consistent positive net CO_2 efflux (Fig. 19C). Diurnal patterns became more clear with higher temperatures from May to October (Fig. 19C) and in this period CO_2 fluxes decreased during the day to sometimes reach net negative fluxes (net uptake of CO_2) during and after midday (Fig. 19C), although the net emissions were also observed in the daytime period (Fig. 19C). The net negative fluxes can likely be explained by photosynthetic activity of aquatic plants on the surface of the ditch or by algae in the water column which was measured due to the transparency of the chamber. Using an opaque chamber instead would likely have resulted in different net CO_2 efflux in daytime. For N_2O, the same pattern as for CH_4 was observed, where flux magnitude across the day fluctuated around zero, except for January where N_2O fluxes were consistently above zero (Fig. 19D).

https://doi.org/10.5194/essd-2025-123
Preprint. Discussion started: 25 March 2025

3.6.3.3 Monthly variability in ditch fluxes

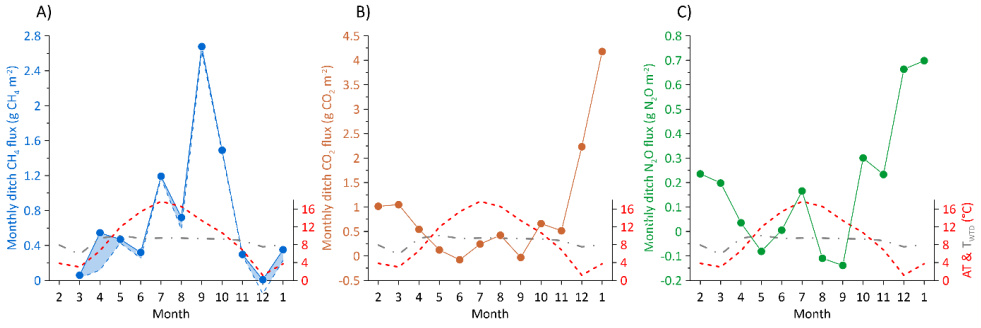

Figure 20: Monthly summed ditch fluxes of A) CH_4 in g CH_4 m^{-2}, B) CO_2 in g CO_2 m^{-2} and C) N_2O in g N_2O m^{-2}. In A) the blue dashed line is the contribution of diffusive fluxes and the shaded blue area between the full and dashed blue lines represent the monthly contribution of ebullition to the total flux. Red and grey dashed lines show the monthly average air (AT) and groundwater temperature (T_{WTD}) in °C, respectively.

The monthly sums of CH_4 show proportionality to air temperature, although peak CH_4 emissions (September) occurred after air temperature peak (July) (Fig. 20A). Diffusive fluxes comprised the major emission pathway of CH_4 in the ditch (between 21% - 99%), with the contribution from ebullition being highest in March (55%) and April (78%) (Fig. 20A). Water temperature in the ditch was relatively stable throughout the year, varying between 5.8 – 10.1°C being highest from April to November and lowest from December to March. However, there is little indication of a direct relation between ditch water temperature and net GHG fluxes (Fig. 20A-C).

For CO_2 and N_2O, the seasonal pattern is reversed with lowest fluxes during the warmest periods, approaching net zero or even net negative fluxes (Fig. 20B and C).

3.6.4 Estimate of the annual soil and ditch GHG budgets at the Vejrumbro location

The GHG flux data was summarized to annual budget for N_2O, CO_2 and CH_4 (Table 3) showing that for the peat soil its gaseous carbon loss was mostly as CO_2, while CH_4 played a negligible role in the C and global warming potential (GWP) budget. The annual soil CO_2 loss of 3,632 g CO_2 m^{-2} y^{-1} is equal to 9.9 tCO_2-C ha^{-1} y^{-1}, which compares well to an estimate of annual soil C loss (8.8 tCO_2-C ha^{-1} y^{-1}) from a drained unfertilized grassland on organic soils in Denmark (Kandel et al., 2018) as well as annual carbon budgets of similar Danish, British and German wetlands (Evans et al., 2021; Koch et al., 2023; Tiemeyer et al., 2020). Annual N_2O emissions were very high (site average: 10.4 g N_2O m^{-2} y^{-1} ranging at this site exceeding previously reported fluxes from this site (1.5 – 2.1 g N_2O m^{-2} y^{-1}) (Nielsen et al., 2024) and German organic soils (0.04 – 6.3 g N_2O m^{-2} y^{-1} for grassland and cropland land uses) (Tiemeyer et al., 2020). The annual N_2O GWP contribution is 47% compared to 53% for CO_2, indicating that N_2O may in fact dominate the GWP budget at this site had gross primary production been included in the measurements. It is important to reiterate here that the flux measurements of this study were done on bare soil whereas the studies referenced above included vegetation. Thus, while we purposely omitted aboveground autotrophic respiration, it cannot be ruled out that living roots inhabited the soil below the chambers and hence contributed to the observed CO_2 emission rates.

https://doi.org/10.5194/essd-2025-123
Preprint. Discussion started: 25 March 2025

The high N_2O fluxes may be a result of high rates of denitrification in the subsoil as NO_3-enriched agricultural runoff from the surrounding intensively cultivated areas, which was not affecting groundwater NO_3^- concentration in the center of the wetland with lower N_2O (Nielsen et al., 2024). The groundwater enters the northern peripheral zone of the wetland at Vejrumbro coinciding with the position of the measurement transect. Although, sporadic measurements of NO_3^- concentrations in groundwater at the SkyLine2D transect did not show elevated NO_3^-, it may be because it was already NO_3^- depleted from denitrification. The lack of consistent hot moments of CH_4 emissions from the soil despite hydrological conditions in the subsoil being conducive for CH_4 production could indicate that redox potential is elevated due to presence of for example NO_3^-. This hypothesis remains to be tested.

Per square meter, the ditch emitted less N_2O and CO_2 than the peat soil, but was a hotspot of CH_4 emission, although annual emissions (10.4 g CH_4 m^{-2} y^{-1}) are lower than previously reported for ditches in peat soil (up to 44 g CH_4 m^{-2} y^{-1}) (Peacock et al., 2021). For the ditch CH_4 budget, ebullition only constitutes 3.7% of annual net CH_4 emissions. This proportion may be underestimated as the count of ebullition events may have been underestimated (Prairie & del Giorgio, 2013).

Table 3: Annual summarized budget of, CO_2 (g CO_2 m^{-2} y^{-1}), CH_4 (g CH_4 m^{-2} y^{-1}) and N_2O (g N_2O m^{-2} y^{-1}) and converted to global warming potential over a 100 year time scale (GWP_{100}) using GWP factors of 273 and 27 for N_2O and CH_4, respectively, for peat soil and the ditch.

Peat soil	CO_2[1]	CH_4[2]	N_2O[2]
Annual sum (g m^{-2} y^{-1})	**3632** [2941;4347]	**0.09** [-0.05;0.22]	**11.6** [9.2;14.1]
GWP100 (tCO_2-eq ha^{-1} y^{-1})	**36** [29;43]	**0.023** [-0.014;0.06]	**32** [25;39]
%GWP	53	0	47
Ditch			
Annual sum (g m^{-2} y^{-1})	**974**	**10.4**	**0.42**
GWP100 (tCO_2-eq ha^{-1} y^{-1})[3]	**9.7**	**2.8** ***(8.7)***	**1.1**
%GWP[3]	70 *(50)*	22 *(44)*	8 *(6)*

[1]$CO_2 = R_h + R_{auto}$. Net ecosystem productivity (NEP) input is not included. [2]Global warming potential (GWP) (100 year) for N_2O = 273 and CH_4 = 27. [3]Budget for 20 years GWP for CH_4 = 84 is shown in parenthesis.

4 Data availability

Data for this publication is available for download via https://doi.org/10.60612/DATADK/BZQ8JE (Skov Nielsen et al. 2025)

https://doi.org/10.5194/essd-2025-123
Preprint. Discussion started: 25 March 2025

5 Conclusion

The dataset presented here is unique for temperate fens and demonstrate the advantage of using automated GHG measurements systems to resolve temporal and spatial patterns of GHG dynamics in high detail. The dataset also links how especial temporal variation of soil hydrology and temperature is linked to the dynamics of fluxes and highlight that spatial variability in hydrology and temperatures not necessarily can be used to predict flux magnitudes within the sites. The cause for the spatial variability of GHG fluxes remains unresolved.

The measurements of the soil GHG fluxes show that the magnitude of annual cumulative CO_2 fluxes are in the same range as in other studies of temperate fens, and that magnitudes are largely governed by the seasonality of WTD and ST. Cumulative soil N_2O fluxes exceed what has been previously reported for temperate fens, but show similar seasonal regulation by ST. However, in contrast to soil CO_2 fluxes, soil N_2O is emitted largely in pulses related to rapid fluctuations of WTD that increase in size with temperature. These measurements therefore point to an important, but difficult to capture dynamic of N_2O in peatlands where hot moments during the warm periods determine most of the annual emissions. A likely cause for the high soil N_2O emissions could be leaching of inorganic nitrogen from surrounding agricultural fields, but this remains to be proven. The site was during measurement period an insignificant source of soil CH_4, which is likely due to the well-drained summer period and a cold wet winter, providing suboptimal conditions for CH_4 production. Soil CO_2 and N_2O fluxes both showed diurnal variability with higher fluxes during midday where the amplitude between night and day was augmented with ST. This was not observed for soil CH_4 fluxes. The ditch at the site was a net source of both N_2O and CO_2, but at rates 27 and 4 times lower than the soil GHG fluxes respectively. However, the ditch acted as a CH_4 source mostly comprised of diffusive emissions from the water surface, but with observations of ebullition.

We wish to publish this dataset to the research community with the intention that experimentalists and modellers can use the data to test hypothesis on basic hydrological and thermal regulation of GHG fluxes and develop models to predict spatiotemporal variability of the GHG fluxes.

Competing interests

The authors declare that they have no conflict of interest.

Author contributions

JRC, PEL and KSL designed the experiment and carried them out. ASN performed flux calculation and quality checking. RJP and PEL installed the equipment for groundwater measurements. All authors contributed to writing of this manuscript.

Acknowledgements

The measurements are the results of the RePeat (grant nr. 33010-NIFA-19-724), INSURE and ReWet (grant nr. 5229-0002b) projects hosted by University of Copenhagen and Aarhus University. ReWet is part of the Danish roadmap for research infrastructure funded by The Danish Agency for Science and Higher Education. INSURE was part of EJP Soil and received funding from the European Union's Horizon 2020 research and innovation programme under the grant agreement no. 862695.

https://doi.org/10.5194/essd-2025-123
Preprint. Discussion started: 25 March 2025

References

Askaer, L., Elberling, B., Friborg, T., Jørgensen, C. J., & Hansen, B. U. (2011). Plant-mediated CH4 transport and C gas dynamics quantified in-situ in a Phalaris arundinacea-dominant wetland. *Plant and Soil*, *343*(1–2), 287–301. https://doi.org/10.1007/s11104-011-0718-x

Brændholt, A., Steenberg Larsen, K., Ibrom, A., & Pilegaard, K. (2017). Overestimation of closed-chamber soil CO2 effluxes at low atmospheric turbulence. *Biogeosciences*, *14*(6), 1603–1616. https://doi.org/10.5194/bg-14-1603-2017

Butterbach-Bahl, K., & Wolf, B. (2017). Warming from freezing soils. *Nature Geoscience*, *10*(4), 248–249. https://doi.org/10.1038/ngeo2915

Evans, C. D., Peacock, M., Baird, A. J., Artz, R. R. E., Burden, A., Callaghan, N., Chapman, P. J., Cooper, H. M., Coyle, M., Craig, E., Cumming, A., Dixon, S., Gauci, V., Grayson, R. P., Helfter, C., Heppell, C. M., Holden, J., Jones, D. L., Kaduk, J., … Morrison, R. (2021). Overriding water table control on managed peatland greenhouse gas emissions. *Nature*, *593*(7860), 548–552. https://doi.org/10.1038/s41586-021-03523-1

Hutchinson, G. L., & Mosier, A. R. (1981). Improved Soil Cover Method for Field Measurement of Nitrous Oxide Fluxes. *Soil Science Society of America Journal*, *45*(2), 311. https://doi.org/10.2136/sssaj1981.03615995004500020017x

Kandel, T. P., Lærke, P. E., & Elsgaard, L. (2018). Annual emissions of CO2, CH4 and N2O from a temperate peat bog: Comparison of an undrained and four drained sites under permanent grass and arable crop rotations with cereals and potato. *Agricultural and Forest Meteorology*, *256–257*, 470–481. https://doi.org/10.1016/j.agrformet.2018.03.021

Koch, J., Elsgaard, L., Greve, M. H., Gyldenkærne, S., Hermansen, C., Levin, G., Wu, S., & Stisen, S. (2023). Water-table-driven greenhouse gas emission estimates guide peatland restoration at national scale. *Biogeosciences*, *20*(12), 2387–2403. https://doi.org/10.5194/bg-20-2387-2023

Kroon, P. S., Hensen, a., Bulk, W. C. M., Jongejan, P. a. C., & Vermeulen, a. T. (2008). The importance of reducing the systematic error due to non-linearity in N2O flux measurements by static chambers. *Nutrient Cycling in Agroecosystems*, *82*(2), 175–186. https://doi.org/10.1007/s10705-008-9179-x

Nielsen, C. K., Liu, W., Koppelgaard, M., & Laerke, P. E. (2024). To Harvest or not to Harvest: Management Intensity did not Affect Greenhouse Gas Balances of Phalaris Arundinacea Paludiculture. *Wetlands*, *44*(6), 79. https://doi.org/10.1007/s13157-024-01830-7

Peacock, M., Audet, J., Bastviken, D., Cook, S., Evans, C. D., Grinham, A., Holgerson, M. A., Högbom, L., Pickard, A. E., Zieliński, P., & Futter, M. N. (2021). Small artificial waterbodies are widespread and persistent emitters of methane and carbon dioxide. *Global Change Biology*, *27*(20), 5109–5123. https://doi.org/10.1111/gcb.15762

https://doi.org/10.5194/essd-2025-123
Preprint. Discussion started: 25 March 2025

Pedersen, A. R., Petersen, S. O., & Schelde, K. (2010). A comprehensive approach to soil-atmosphere trace-gas flux estimation with static chambers. *European Journal of Soil Science*, *61*(6), 888–902. https://doi.org/10.1111/j.1365-2389.2010.01291.x

Pihlatie, M. K., Christiansen, J. R., Aaltonen, H., Korhonen, J. F. J., Nordbo, A., Rasilo, T., Benanti, G., Giebels, M., Helmy, M., Sheehy, J., Jones, S., Juszczak, R., Klefoth, R., Lobo-do-Vale, R., Rosa, A. P., Schreiber, P., Serça, D., Vicca, S., Wolf, B., & Pumpanen, J. (2013). Comparison of static chambers to measure CH4 emissions from soils. *Agricultural and Forest Meteorology*, *171–172*, 124–136. https://doi.org/10.1016/j.agrformet.2012.11.008

Prairie, Y. T., & del Giorgio, P. A. (2013). A new pathway of freshwater methane emissions and the putative importance of microbubbles. *Inland Waters*, *3*(3), 311–320. https://doi.org/10.5268/IW-3.3.542

Pullens, J. W. M., Abalos, D., Petersen, S. O., & Pedersen, A. R. (2023). Identifying criteria for greenhouse gas flux estimation with automatic and manual chambers: A case study for <scp> N $_2$ O </scp>. *European Journal of Soil Science*, *74*(1). https://doi.org/10.1111/ejss.13340

Reza Mashhadi, S., Grombacher, D., Zak, D., Erik Lærke, P., Estrup Andersen, H., Christian Hoffmann, C., & Jes Petersen, R. (2024). Borehole nuclear magnetic resonance as a promising 3D mapping tool in peatland studies. *Geoderma*, *443*, 116814. https://doi.org/10.1016/j.geoderma.2024.116814

Rheault, K., Christiansen, J. R., & Larsen, K. S. (2024). goFlux: A user-friendly way to calculate GHG fluxes yourself, regardless of user experience. *Journal of Open Source Software*, *9*(96), 6393. https://doi.org/10.21105/joss.06393

Skov Nielsen, A., Larsen, K.S., Lærke, P.E., Rodriguez, A.F., Pullens, J.W.M., Petersen, R.J., Christiansen, J.R. (2025), "Supporting Data for: A full year of continuous net soil and ditch CO2, CH4, N2O fluxes, soil hydrology and meteorology for a drained fen in Denmark", https://doi.org/10.60612/DATADK/BZQ8JE, DeiC Dataverse, Denmark.

Sø, J. S., Sand-Jensen, K., Martinsen, K. T., Polauke, E., Kjær, J. E., Reitzel, K., & Kragh, T. (2023). Methane and carbon dioxide fluxes at high spatiotemporal resolution from a small temperate lake. *Science of The Total Environment*, *878*, 162895. https://doi.org/10.1016/j.scitotenv.2023.162895

Thers, H., Knudsen, M. T., & Lærke, P. E. (2023). Comparison of GHG emissions from annual crops in rotation on drained temperate agricultural peatland with production of reed canary grass in paludiculture using an LCA approach. *Heliyon*, *9*(6), e17320. https://doi.org/10.1016/J.HELIYON.2023.E17320

Tiemeyer, B., Freibauer, A., Borraz, E. A., Augustin, J., Bechtold, M., Beetz, S., Beyer, C., Ebli, M., Eickenscheidt, T., Fiedler, S., Förster, C., Gensior, A., Giebels, M., Glatzel, S., Heinichen, J., Hoffmann, M., Höper, H., Jurasinski, G., Laggner, A., … Drösler, M. (2020). A new methodology for organic soils in national greenhouse gas inventories: Data synthesis, derivation and application. *Ecological Indicators*, *109*, 105838. https://doi.org/10.1016/j.ecolind.2019.105838

https://doi.org/10.5194/essd-2025-123
Preprint. Discussion started: 25 March 2025

669 Wik, M., Varner, R. K., Anthony, K. W., MacIntyre, S., & Bastviken, D. (2016). Climate-sensitive northern
670 lakes and ponds are critical components of methane release. *Nature Geoscience*, *9*(2), 99–105.
671 https://doi.org/10.1038/ngeo2578

672 Wilson, S. J., Bond-Lamberty, B., Noyce, G., Bittencourt Peixoto, R., & Megonigal, J. P. (2024). fluxfinder: An
673 R Package for Reproducible Calculation and Initial Processing of Greenhouse Gas Fluxes From Static
674 Chamber Measurements. *Journal of Geophysical Research: Biogeosciences*, *129*(11).
675 https://doi.org/10.1029/2024JG008208

676